Growth-temperature dependence of conductivity at the $LaCrO_3/SrTiO_3$ (001) interface

Athby Al-Tawhid, Jordan R. Frick, Daniel B. Dougherty, and Divine P. Kumah

Citation: Journal of Vacuum Science & Technology A **37**, 021102 (2019); doi: 10.1116/1.5085334
View online: https://doi.org/10.1116/1.5085334
View Table of Contents: https://avs.scitation.org/toc/jva/37/2
Published by the American Vacuum Society

Growth-temperature dependence of conductivity at the $LaCrO_3/SrTiO_3$ (001) interface

Athby Al-Tawhid, Jordan R. Frick, Daniel B. Dougherty, and Divine P. Kumah[a)]
Department of Physics, North Carolina State University, Raleigh, North Carolina 27695

(Received 11 December 2018; accepted 4 February 2019; published 20 February 2019)

The effect of growth conditions and postgrowth treatment on the structural and electronic properties of the polar/nonpolar $LaCrO_3/SrTiO_3$ (LCO/STO) interface has been investigated. Under low oxygen partial pressure, oxygen vacancies are formed in the STO substrate resulting in metallicity with a measured sheet carrier concentration of $10^{16}\,cm^{-2}$. Annealing postgrowth in flowing oxygen causes the sheet carrier concentration to saturate to $10^{13}\,cm^{-2}$, which is consistent with the reported values of a two-dimensional gas at other polar/STO interfaces. However, growth under nonreducing growth conditions leads to insulating behavior. High-resolution synchrotron x-ray-based structural determination of the atomic-scale structures of both metallic and insulating LCO/STO interfaces shows chemical intermixing and an interfacial lattice expansion. *Published by the AVS.*
https://doi.org/10.1116/1.5085334

I. INTRODUCTION

Polar/nonpolar perovskite interfaces have attracted considerable interest since the discovery of novel interfacial phenomena not found in the constituent bulk materials.[1–4] Of considerable interest is the interface between polar $LaAlO_3$ (LAO) and nonpolar $SrTiO_3$ (STO), which exhibits a high mobility quasi-two-dimensional electron gas (q-2-deg), ferromagnetism, and superconductivity, despite both materials being nonmagnetic bulk insulators.[1,2,5] Conductivity at the LAO/STO interface has been attributed to an interfacial polarity driven electronic reconstruction,[1] ionic intermixing[6] and defects related to cation nonstoichiometry,[7] and oxygen vacancies.[8] Since its discovery, other complex oxides such as $SmTiO_3$, $GdTiO_3$, $LaTiO_3$, $LaGaO_3$, $LaVO_3$, and $NdTiO_3$ have been grown on STO and have been shown to also exhibit interfacial conductivity,[9–16] while some polar/nonpolar interfaces such as the $LaCrO_3$ (LCO)/STO were found to be insulating.[17] An electric field at the LCO/STO interface observed by photoelectron spectroscopy[17] is expected to result in an electronic reconstruction resulting in a conducting interface. The absence of conductivity is attributed to Ti outdiffusion, which results in a redistribution of charge in the interfacial CrO_2 layers.[17] However, mobile charge carriers have been reported for LCO/STO superlattices.[18] To gain further insight into the intrinsic and extrinsic mechanisms that trigger conduction at these interfaces, the effect of growth conditions is required.

In this paper, we investigate the effect of growth temperature and postgrowth treatment on the electrical and structural properties of the LCO/STO interface using a combination of high-resolution synchrotron x-ray diffraction structural measurements, angle-resolved photoemission spectroscopy (ARPES), and temperature-dependent transport measurements. Previous reports on the LAO/STO interface have shown that growth temperature can have a considerable effect on the transport properties of the interface.[19] Here, we find that by varying the growth temperature and postgrowth treatments, the interface can be tuned from an insulating to a high mobility metallic state. Samples grown at a lower temperature (600 °C) are insulating while higher growth temperatures (800 °C) under identical oxygen pressures lead to metallicity. The as-grown sample exhibits sheet carrier concentration on the order of $10^{16}\,cm^{-2}$ which is similar to that of LAO/STO interfaces under similar growth conditions as well as oxygen reduced STO.[20] Annealing the metallic samples in flowing oxygen causes the reduction in the sheet carrier concentrations to $10^{13}\,cm^{-2}$, as well as a change in color from gray to clear, which we attribute to the reduction of oxygen vacancy concentration in the bulk STO. There is an expansion of the out-of-plane lattice constant of the STO at the interface in both samples which we attribute to the La–Sr interdiffusion. The necessity of a reducing environment for the interfacial conductivity to occur points to defects related to oxygen vacancies as the origin of the interfacial metallicity.[18]

II. EXPERIMENTAL METHODS

A. Growth and treatment

LCO films with a nominal thickness of 10 unit cells (uc) were grown on (001) oriented STO substrates by molecular beam epitaxy (MBE). Prior to growth, the STO substrates were treated with buffered HF and annealed in flowing oxygen at 1000 °C in a tube furnace for 2 h to create a Ti terminated surface.[21] Atomic force microscope (AFM) images of the substrate after treatment show that the terrace step structure is present. The LCO films were grown at 1×10^{-7} Torr oxygen partial pressure with the base pressure of the MBE chamber being 2×10^{-10} Torr. The flux of the La and Cr sources was calibrated before growth with a quartz crystal microbalance. *In situ* reflection high energy electron diffraction (RHEED) was used to monitor the growth process. Images of the RHEED pattern of a bare STO and a 10 uc LCO are shown in Figs. 1(a) and 1(b), respectively. RHEED oscillations of a 10 uc LCO in Fig. 1(c) indicate that layer-by-layer growth is

Note: This paper is part of the Special Topic Collection on Complex Oxides.
a)Electronic mail: dpkumah@ncsu.edu

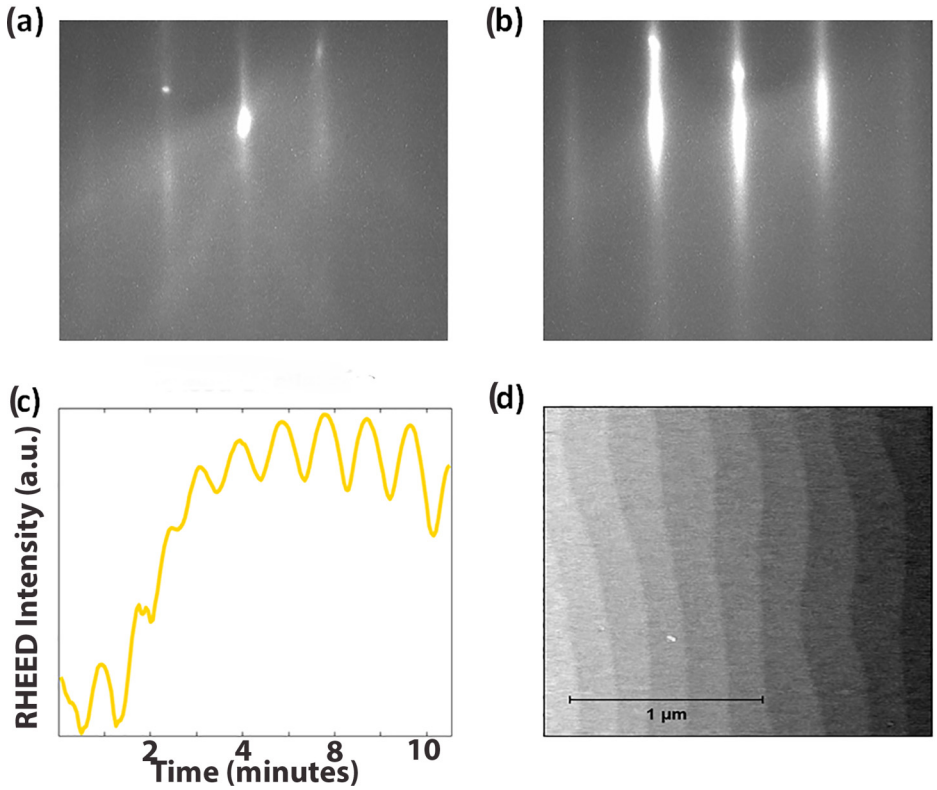

FIG. 1. Growth properties of LCO films grown on STO by molecular beam epitaxy. (a) RHEED image of the bare STO substrate. (b) RHEED image 10 uc LCO on STO after growth and (c) RHEED oscillations for a 10 uc LCO film grown at 800 °C and 1×10^{-7} Torr O_2. (d) AFM image of a 10 uc LCO. Note that the terrace step structure is preserved with a step height of 4 Å.

achieved, and the number of layers deposited is determined by the number of RHEED oscillations. AFM images after growth of the LCO [Fig. 1(d)] show that the terrace step structure of the STO substrate is preserved confirming epitaxial growth. The samples were grown in two temperature regimes; a high temperature regime (800 °C) (henceforth referred to as HT) and a low temperature regime (600 °C) (henceforth referred to as LT). The HT samples were then split into two groups; a set of samples that were annealed *ex situ* in a tube furnace at 400 °C with flowing pure (99%) oxygen for 4 h and a second set that was left untreated.

B. Transport/Hall measurements

Temperature-dependent Hall and resistivity measurements were performed using a 4-point Van der Pauw configuration in the range of 2–300 K. Gold contacts were deposited at the corners of the samples using a shadow mask. All transport measurements were performed using a Quantum Design physical property measurement system. Both as-grown and annealed samples were found to be metallic at room temperature with sheet resistivities on the order of 100 and 30 kΩ/□, respectively. The LT samples were too insulating to measure their sheet resistance which we estimate to be greater than 100 MΩ/□.

C. Synchrotron x-ray diffraction

To determine the differences in the atomic-scale structures of the as-grown HT-metallic and LT-insulating nominally 10 uc LCO films, synchrotron x-ray diffraction measurements were carried out at the 33ID beamline at the Advanced Photon Source. Crystal truncation rods (CTRs)[22] were measured along the STO bulk crystallographic directions with an incident x-ray energy of 15.5 eV. The layer-resolved structure and the composition of the films were obtained from fitting the CTR data with a genetic-based algorithm, GenX.[23] The parameters of the fit included the out-of-plane lattice constant of each layer, Debye-Waller factors for each element, and the fractional occupation of the surface LCO layer to account for surface roughness. Additionally, the chemical composition of the first five layers of the film and the substrate at the film/substrate interface were optimized to allow for intermixing. Each element was also allowed to displace in the (001) direction, and the oxygen octahedral was allowed to rotate and tilt.[24,25] The fit was then compared to the data iteratively to minimize the error between them. Structural convergence was achieved by minimizing the crystallographic R1 error function. We obtain excellent fits with figures of merit values below 0.08 for each fit. Representative measured CTRs and their associated fits for the HT and LT as-grown samples are shown in Figs. 2(a) and 2(b), respectively.

D. Angle-resolved photoemission spectroscopy

To determine if the changes to conductivity were related to changes in the electronic structure of the LCO films,

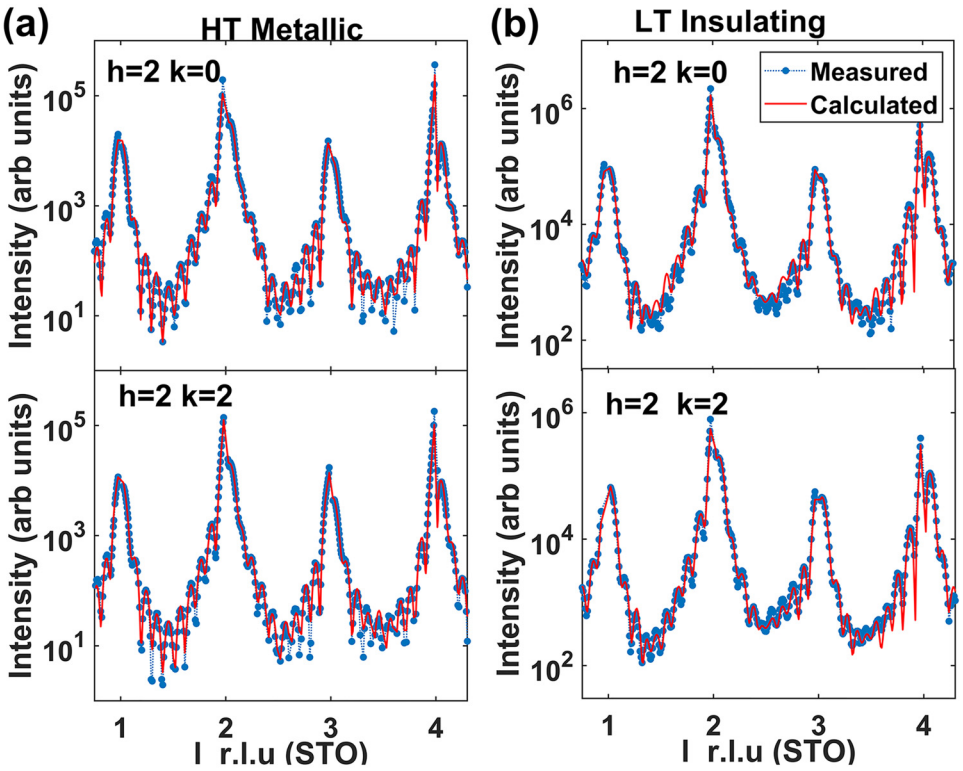

FIG. 2. Representative measured and calculated CTRs for (a) an HT as-grown 10 uc LCO/STO heterostructure grown at 800 °C and (b) an LT as-grown 10 uc LCO/STO heterostructure grown at 600 °C. The h, k, and l values are in units of the bulk cubic $SrTiO_3$ reciprocal lattice vectors.

ARPES was performed at room temperature (27 °C) in ultra-high vacuum using both an He I (21.2 eV) plasma light source and a pulsed laser source (6.2 eV from the fourth harmonic of a Ti-sapphire laser). Photoelectrons were analyzed using a 150 mm mean radius hemispherical analyzer (Specs Phoibos 150) with a 2D detector. All samples were transported from the growth chamber through ambient air to be inserted in the ARPES chamber. They were subsequently annealed in vacuum at 300 °C for 30 min and allowed to cool back to room temperature prior to data collection. The binding energy scale on all samples was corrected for charging effects in order to correspond with Maiti and Sarma.[26]

III. RESULTS AND DISCUSSION

To determine the effect of the growth conditions on the structural properties of the LCO/STO interface, the layer-resolved atomic-scale structures were determined from fits to CTRs measured by synchrotron x-ray diffraction. The structural properties of as-grown HT and LT samples are compared in Fig. 3. Figure 3(a) shows the A-site composition along the growth direction for the LT and HT samples. The chemical profile across the interface shows that significant La/Sr interdiffusion occurs for both insulating and metallic samples in agreement with previous electron microscopy and Rutherford backscattering measurements which has been suggested to be driven by strain relaxation.[27] For both the HT and LT samples, a tail of Sr outdiffusion into the LCO film extends about 4–5 layers away from the interface [layers 1–5 of Fig. 3(a)] decaying from 25% in the first interfacial LCO layer. Due to the comparable atomic scattering factors of Cr (24 electrons) and Ti (22 electrons) at 15.5 keV and the ability of the B cations to occupy different oxidation states, the uncertainty associated with the B-site composition profile is too large to draw relevant conclusions. However, previous high-resolution electron microscopy measurements show Cr–Ti interdiffusion occurring at the LCO/STO interface.[27,28]

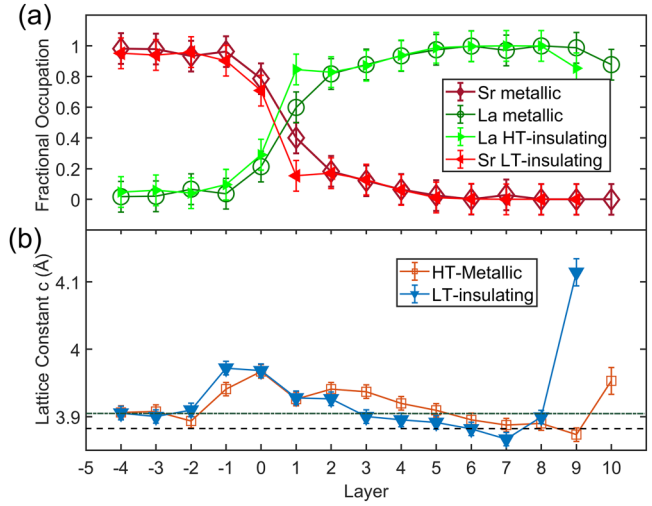

FIG. 3. (a) Layer-resolved Sr/La occupation for metallic as 800 °C and insulating 600 °C as-grown LCO samples. (b) Layer-resolved out-of-plane lattice constant for metallic as 800 °C and insulating 600 °C as-grown LCO samples. Layer 0 indicates the top of the STO substrate. The expected out-of-plane lattice constants of STO (3.905 Å) and LCO (3.88 Å) are indicated by horizontal lines on the plot.

The layer-resolved lattice constants shown in Fig. 3(b) are determined from the spacing of the A-site cations along the growth direction. We observe in both samples an expansion at the interface followed by a linear decrease toward the film surface. The expansion in the STO (layers −1 and 0) which is also observed in LAO/STO interfaces is related to the diffusion of La into the STO substrate.[6,24] La substituting for Sr would donate an electron and alter the valence state of Ti from +4 to +3 increasing its ionic radius. For stochiometrtic LCO films coherently strained to STO, the expected out-of-plane lattice constant is 3.88 Å for an LCO Poisson ratio of 0.23.[28] The larger lattice constant in both the HT-metallic and the LT-insulating LCO film may be related to La–Sr and Cr–Ti interdiffusion and/or oxygen vacancies in the LCO. The HT as-grown samples show a larger average lattice constant which is likely due to the higher concentration of oxygen vacancies.[29,30] In both samples, we observe a large lattice expansion at the film surface which is likely due to structural distortions and the polar discontinuity at the film vacuum interface.[24]

Figure 4 shows the temperature-dependent mobility (μ), sheet resistance, and sheet carrier density (n_s) for the LCO/STO samples determined from the Hall measurements. The transport properties are compared for the HT as-grown and postgrowth annealed samples. The as-grown sample shows a sheet carrier density of $10^{16}\,cm^{-2}$, which indicates that the majority of the carrier are found in the reduced STO substrate.[20] This is corroborated by the fact that the temperature dependence of the sheet resistance and mobility is similar to previous reports of reduced STO and LAO/STO interfaces grown under low oxygen growth pressures without postgrowth annealing.[1,20] Upon annealing, the oxygen vacancies are reduced, and the sheet carrier concentration saturates to approximately $10^{13}\,cm^{-2}$. The temperature dependence of the sheet resistance reduces, and a minimum occurs at 30 K followed by an upturn. The upturn at low temperatures is possibly due to weak localization or Kondo scattering. The source of Kondo scattering may be either magnetic Ti3+ or Cr.[16,31–33] These results are similar to LAO/STO heterostructures which have been grown under the reducing condition and then annealed post growth in an oxygen-rich environment or grown at high oxygen partial pressure.[20,31]

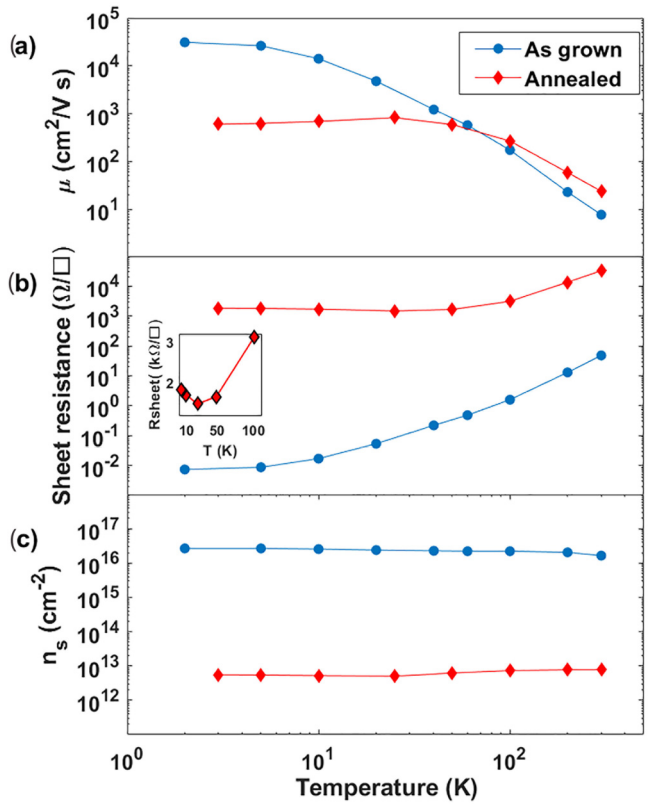

FIG. 4. (a) Comparison of mobility, μ, (b) sheet resistance, and (c) sheet carrier density, n_s, as a function of temperature for a 10 uc LCO/STO grown at 800 °C without a postgrowth anneal and a 10 uc LCO/STO grown at 800 °C followed by an anneal in 1 atm 99.99% O_2 at 400 °C for 4 h. The inset shows sheet resistance of the annealed sample at low temperature to highlight the upturn.

In contrast, the LT samples were found to be completely insulating with RT sheet resistances greater than 100 MΩ/□. This result is similar to previous reports of LCO/STO heterostructure grown at 650 °C and 6×10^{-8} Torr partial oxygen pressure.[17,28] Annealing LT samples in the growth conditions of HT samples (10^{-7} Torr partial O_2 pressure and 800 °C) causes a high concentration of oxygen vacancies to form in the STO substrate as evidenced by its high sheet carrier concentration ($10^{16}\,cm^{-2}$) as well as a gray discoloration of the sample. However, upon annealing the sample in flowing oxygen at 400 °C, the sample returns to its previous insulating state. This result suggests that reducing conditions are necessary during the growth of interfacial conductivity to occur.

The necessity of the reducing condition (high temperature and low oxygen partial pressure) during growth suggests that oxygen vacancies in either the STO or the LCO play an important role in the formation of the 2-deg. Doping due to cation intermixing can be ruled out as the main source of conductivity as it is observed in both the insulating and metallic samples in Fig. 4. Hole doping of LCO with Sr can induce an insulator-metal transition for Sr dopants above 65%.[34] However, the Sr content observed for both films in Fig. 3(a) is insufficient to account for the metallicity. Additionally, the Hall coefficient for the metallic samples is negative indicative of majority electron carriers.

Angle-resolved photoelectron spectroscopy measurements were carried out to elucidate the electronic structure near the surface of the $LaCrO_3$ films. Figure 5(a) shows ARPES measurements of a 4 unit cell $LaCrO_3$ film grown under high temperature conditions that was verified by resistivity measurements to show metallic behavior. Between 1 eV and 2 eV, we find a state assigned predominantly to the Cr 3d valence orbitals, while the more deeply bound state (2.5–4.0 eV) comes predominantly from O 2p orbitals.[26] The data shown in Figs. 5(a) and 5(b) are representative of all films studied under different thicknesses, different photon energies, and different substrate temperatures during growth. Despite these numerous different conditions, all ARPES measurements showed precisely the features seen in Fig. 5(a). No photoelectron intensity near the Fermi level (0.0 eV) is observed for any

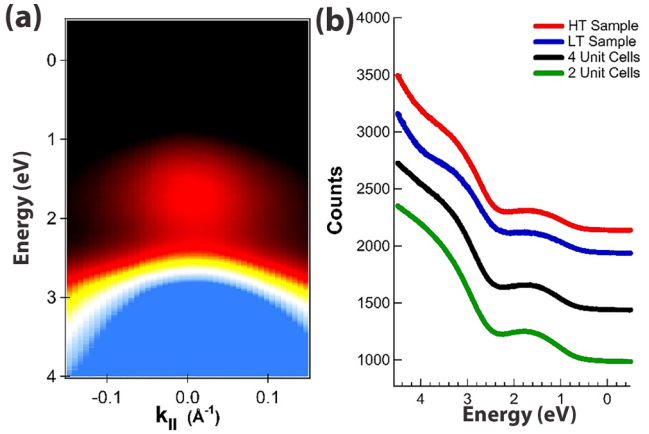

FIG. 5. (a) Angle-resolved photoemission spectra of 4 unit cell HT $LaCrO_3$ thin film; (b) line cuts at $k = 0$ of a thick (bulk-like) HT $LaCrO_3$ sample, thick LT sample, 4 unit cell thick HT sample, and 2 unit cell HT sample. The line cuts are stacked vertically for clarity.

of the LCO films considered [Fig. 5(b)]. Some minor differences in the valence band spectra may exist due to the differences in the secondary electron background and in the defect density between the films. Nevertheless, the photoemission observations show that the electron structure near the surfaces of each film is essentially identical. The results shown in Fig. 5 correspond to 21.2 eV photon energies, which result in photoelectrons with very short escape depths, and thus sensitive mostly to the surface of the film. By extending our measurements down to 2 unit cell films [lowest spectrum in Fig. 5(b)], we confirm that the metallic transport behavior is not occurring in the LCO film.

A possible mechanism responsible for the formation of the 2-deg at the HT LCO/STO interface involves the formation of oxygen vacancies at the LCO/STO interface, the bulk STO substrate, and the LCO film as evidenced by the high sheet carrier concentration (10^{16} cm^{-2}) and the expansion of the LCO lattice. Here, oxygen vacancies form during growth due to a redox reaction between the oxygen-deficient LCO film and the STO substrate and are stabilized at the interface.[35,36] Upon annealing in oxygen, oxygen vacancies in the bulk STO and film are removed, while at the interface, the vacancies are trapped. For amorphous LAO films grown on the STO under reducing growth conditions, a redox reaction between the film and the TiO_2-terminated STO surface has been proposed to result in oxygen vacancies in the STO layers close to the interface which contributes to metallicity.[37]

To verify the necessity for the reducing conditions for interfacial metallicity, we grew an insulating sample under oxidizing conditions. For growth under low temperature, the redox reaction is suppressed resulting in an insulating interface.[28,36] This sample was annealed in vacuum resulting in metallicity with a sheet carrier concentration of 10^{16} cm^{-2} indicative of bulk metallicity. A postanneal in oxygen at 400 °C resulted in insulating transport behavior. We note that additional mechanisms including charge transfer induced by the oxygen vacancies may contribute to the interfacial conductivity and further studies are required to elucidate their role.[20,37–39]

IV. CONCLUSION

In summary, we have shown that growth conditions play a critical role in the creation of mobile charge carriers in LCO/STO(001) heterostructures. Under nonreducing conditions, both the substrate and the film are completely insulating. Under reducing conditions (high growth temperature, low oxygen pressure), oxygen vacancies form in the bulk STO as evidenced by high sheet carrier concentrations. However, postgrowth annealing in pure oxygen at 400 °C causes a reduction in the oxygen vacancies and a sheet carrier concentration that saturates to approximately 10^{13} cm^{-2}. The electrical properties of the LCO/STO interface show remarkable similarities to the 2-deg at the LAO/STO interface, suggesting that they share a common origin. Structurally, both insulating and metallic LCO/STO samples exhibit significant La/Sr intermixing and an expansion of the out-of-plane lattice constant at the interface. The HT samples show a larger average lattice constant in the film suggesting a higher concentration of point defects, most likely in the form of oxygen vacancies. Further work is required to investigate the effect of the proximity of antiferromagnetic LCO (Refs. 40–42) on the magnetoresistance and superconductivity[5] observed at polar oxide/STO interfaces.

ACKNOWLEDGMENTS

This material is based upon work supported by the National Science Foundation under Grant No. NSF DMR1751455. Photoelectron spectroscopy experiments were supported by U.S. Department of Energy, Office of Science, Basic Energy Sciences under Award No. DE-SC0010324. The use of the Advanced Photon Source was supported by the U.S. Department of Energy, Office of Science, Office of Basic Energy Sciences, under Contract No. DE-AC02-06CH11357.

[1]A. Ohtomo and H. Hwang, Nature **427**, 423 (2004).
[2]A. Brinkman *et al.*, Nat. Mat. **6**, 493 (2007).
[3]F. J. Wong, S.-H. Baek, R. V. Chopdekar, V. V. Mehta, H.-W. Jang, C.-B. Eom, and Y. Suzuki, Phys. Rev. B **81**, 161101 (2010).
[4]J. Mannhart and D. Schlom, Science **327**, 1607 (2010).
[5]N. Reyren *et al.*, Science **317**, 1196 (2007).
[6]P. Willmott *et al.*, Phys. Rev. Lett. **99**, 155502 (2007).
[7]E. Breckenfeld, N. Bronn, J. Karthik, A. Damodaran, S. Lee, N. Mason, and L. Martin, Phys. Rev. Lett. **110**, 196804 (2013).
[8]G. Herranz *et al.*, Phys. Rev. Lett. **98**, 216803 (2007).
[9]P. Perna *et al.*, Appl. Phys. Lett. **97**, 152111 (2010).
[10]P. Moetakef, Appl. Phys. Lett. **99**, 232116 (2011).
[11]L. Kornblum, E. N. Jin, D. P. Kumah, A. T. Ernst, C. C. Broadbridge, C. H. Ahn, and F. J. Walker, Appl. Phys. Lett. **106**, 201602 (2015).
[12]P. B. Marshall, E. Mikheev, S. Raghavan, and S. Stemmer, Phys. Rev. Lett. **117**, 046402 (2016).
[13]C. He, T. Sanders, M. Gray, F. Wong, V. Mehta, and Y. Suzuki, Phys. Rev. B **86**, 081401 (2012).
[14]K. Ahmadi-Majlan *et al.*, Appl. Phys. Lett. **112**, 193104 (2018).
[15]P. Xu, T. C. Droubay, J. S. Jeong, K. A. Mkhoyan, P. V. Sushko, S. A. Chambers, and B. Jalan, Adv. Mater. Interfaces **3**, 1500432 (2016).
[16]P. Xu, Y. Ayino, C. Cheng, V. S. Pribiag, R. B. Comes, P. V. Sushko, S. A. Chambers, and B. Jalan, Phys. Rev. Lett. **117**, 106803 (2016).
[17]S. A. Chambers, L. Qiao, T. C. Droubay, T. C. Kaspar, B. W. Arey, and P. Sushko, Phys. Rev. Lett. **107**, 206802 (2011).
[18]R. B. Comes, S. R. Spurgeon, D. M. Kepaptsoglou, M. H. Engelhard, D. E. Perea, T. C. Kaspar, Q. M. Ramasse, P. V. Sushko, and S. A. Chambers, Chem. Mater. **29**, 1147 (2017).

[19]A. Fête, C. Cancellieri, D. Li, D. Stornaiuolo, A. Caviglia, S. Gariglio, and J.-M. Triscone, Appl. Phys. Lett. **106**, 051604 (2015).
[20]A. Kalabukhov, R. Gunnarsson, J. Börjesson, E. Olsson, T. Claeson, and D. Winkler, Phys. Rev. B **75**, 121404 (2007).
[21]M. Kawasaki, K. Takahashi, T. Maeda, R. Tsuchiya, M. Shinohara, O. Ishiyama, T. Yonezawa, M. Yoshimoto, and H. Koinuma, Science **266**, 1540 (1994).
[22]I. Robinson and D. Tweet, Rep. Prog. Phys. **55**, 599 (1992).
[23]M. Björck and G. Andersson, J. Appl. Crystallogr. **40**, 1174 (2007).
[24]S. Koohfar, A. Disa, M. Marshall, F. Walker, C. Ahn, and D. Kumah, Phys. Rev. B **96**, 024108 (2017).
[25]T. Chen, K. Ahmadi-Majlan, Z. H. Lim, Z. Zhang, J. H. Ngai, A. F. Kemper, and D. P. Kumah, Appl. Phys. Lett. **113**, 201601 (2018).
[26]K. Maiti and D. Sarma, Phys. Rev. B **54**, 7816 (1996).
[27]R. Colby, L. Qiao, K. Zhang, V. Shutthanandan, J. Ciston, B. Kabius, and S. A. Chambers, Phys. Rev. B **88**, 155325 (2013).
[28]L. Qiao, T. C. Droubay, M. E. Bowden, V. Shutthanandan, T. C. Kaspar, and S. A. Chambers, Appl. Phys. Lett. **99**, 061904 (2011).
[29]D. Marrocchelli, N. H. Perry, and S. R. Bishop, Phys. Chem. Chem. Phys. **17**, 10028 (2015).
[30]C. Cazorla, Phys. Rev. Appl. **7**, 044025 (2017).
[31]K. Han *et al.*, Sci. Rep. **6**, 25455 (2016).
[32]H. Xue *et al.*, Phys. Rev. B **98**, 085305 (2018).
[33]S. Das, A. Rastogi, L. Wu, J.-C. Zheng, Z. Hossain, Y. Zhu, and R. Budhani, Phys. Rev. B **90**, 081107 (2014).
[34]K. Zhang, Y. Du, P. Sushko, M. E. Bowden, V. Shutthanandan, S. Sallis, L. F. Piper, and S. A. Chambers, Phys. Rev. B **91**, 155129 (2015).
[35]Y. Chen *et al.*, Nat. Commun. **4**, 1371 (2013).
[36]Q. Fu and T. Wagner, Surf. Sci. **601**, 1339 (2007).
[37]Y. Chen, N. Pryds, J. E. Kleibeuker, G. Koster, J. Sun, E. Stamate, B. Shen, G. Rijnders, and S. Linderoth, Nano Lett. **11**, 3774 (2011).
[38]Y. Li, S. N. Phattalung, S. Limpijumnong, J. Kim, and J. Yu, Phys. Rev. B **84**, 245307 (2011).
[39]Z. Liu *et al.*, Phys. Rev. X **3**, 021010 (2013).
[40]I. Weinberg and P. Larssen, Nature **192**, 445 (1961).
[41]K. Ueda, H. Tabata, and T. Kawai, Science **280**, 1064 (1998).
[42]J.-S. Zhou, J. Alonso, A. Muonz, M. Fernández-Díaz, and J. Goodenough, Phys. Rev. Lett. **106**, 057201 (2011).